Mammalian face as an evolutionary novelty

Hiroki Higashiyama[a,1], Daisuke Koyabu[b,c], Tatsuya Hirasawa[d,e], Ingmar Werneburg[f,g], Shigeru Kuratani[e,h], and Hiroki Kurihara[a]

[a]Department of Physiological Chemistry and Metabolism, Graduate School of Medicine, The University of Tokyo, Tokyo 113-0033, Japan; [b]Jockey Club College of Veterinary Medicine and Life Sciences, City University of Hong Kong, Kowloon, Hong Kong; [c]Research and Development Center for Precision Medicine, University of Tsukuba, 1-2 Kasuga, Tsukuba 305-8550, Japan; [d]Department of Earth and Planetary Science, Graduate School of Science, The University of Tokyo, Tokyo 113-0033, Japan; [e]Evolutionary Morphology Laboratory, RIKEN Cluster for Pioneering Research, Kobe 650-0047, Japan; [f]Senckenberg Centre for Human Evolution and Palaeoenvironment, Eberhard Karls Universität Tübingen, Tübingen 72076, Germany; [g]Fachbereich Geowissenschaften, Eberhard Karls Universität Tübingen, Tübingen 72074, Germany; and [h]Laboratory for Evolutionary Morphology, RIKEN Center for Biosystems Dynamics Research, Kobe 650-0047, Japan

Edited by Neil H. Shubin, University of Chicago, Chicago, IL, and approved September 8, 2021 (received for review June 28, 2021)

The anterior end of the mammalian face is characteristically composed of a semimotile nose, not the upper jaw as in other tetrapods. Thus, the therian nose is covered ventrolaterally by the "premaxilla," and the osteocranium possesses only a single nasal aperture because of the absence of medial bony elements. This stands in contrast to those in other tetrapods in whom the premaxilla covers the rostral terminus of the snout, providing a key to understanding the evolution of the mammalian face. Here, we show that the premaxilla in therian mammals (placentals and marsupials) is not entirely homologous to those in other amniotes; the therian premaxilla is a composite of the septomaxilla and the palatine remnant of the premaxilla of nontherian amniotes (including monotremes). By comparing topographical relationships of craniofacial primordia and nerve supplies in various tetrapod embryos, we found that the therian premaxilla is predominantly of the maxillary prominence origin and associated with mandibular arch. The rostral-most part of the upper jaw in nonmammalian tetrapods corresponds to the motile nose in therian mammals. During development, experimental inhibition of primordial growth demonstrated that the entire mammalian upper jaw mostly originates from the maxillary prominence, unlike other amniotes. Consistently, cell lineage tracing in transgenic mice revealed a mammalian-specific rostral growth of the maxillary prominence. We conclude that the mammalian-specific face, the muzzle, is an evolutionary novelty obtained by overriding ancestral developmental constraints to establish a novel topographical framework in craniofacial mesenchyme.

evolution | craniofacial | skull | mammals

In the movie *For Whom the Bell Tolls* (1943, Paramount), a girl says, "I do not know how to kiss, or I would kiss you. Where do the noses go?" (1) Nothing could reveal more vividly the curious morphological fact that it is the nose, not the tip of the upper jaw, that is the most protruding part of the mammalian face. Therian mammals are thus characterized by a protruding nose, representing a morphologically and functionally semi-independent module for tactile sensory detection and for mammalian olfactory function (Fig. 1*A*) (2–7). The topographical relationship between the nose and cranial bones also shows an exceptional pattern in mammals: the rostral-most bone of the upper jaw, or premaxilla, is found on the ventrolateral sides of the external nostrils in therian mammals, unlike in other amniotes in whom the premaxilla covers the rostromedial tip of the snout (Fig. 1 *A* and *B*) (2–4, 7, 8). However, the evolutionary origin of this therian-specific face (the so-called muzzle) and homology of the therian premaxilla (also known as the incisive bone) have not been examined for a long time (2–4, 7–9).

During vertebrate embryogenesis, the upper jaw is primarily formed by growth of the maxillary prominence of the mandibular arch, except for the premaxilla, the rostral midline part of the upper jaw, which develops by the convergence of the premandibular ectomesenchyme (frontonasal prominence) that initially develops rostral to the mandibular arch ectomesenchyme (Fig. 1*B*) (4, 10–12). This topographical configuration is recognized even in some placoderms; that is, the basic pattern of jaw morphology is thought to be constrained among the jawed vertebrates (12–14). However, the topographical position of the therian premaxilla suggests that this highly conserved pattern is disrupted in mammals in association with the evolution of the mammalian muzzle. Specifically, the innervation pattern of the homonymous "premaxilla" is significantly different in mammals (15), which is also suggestive of fundamental embryological changes.

In the present study, we conducted comparative experimental embryological analyses and cell lineage tracing of the facial primordia to investigate the origin of the mammalian face.

Results

Comparative Embryology. To clarify the topographical positions of the premaxillae, we first compared the embryonic developmental patterns in the frog (*Rana japonica*), gecko (*Paroedura picta*), echidna (*Tachyglossus aculeatus*), and mouse (*Mus musculus*) (Fig. 1*C* and *SI Appendix*, Fig. S1). In the nontherian (frog, gecko, and echidna) embryos, the premaxilla initially ossifies medially to the external nostril, rostrally to the nasal septum, and, in particular, rostroventrally to the solum nasi of

Significance

The anatomical framework of the jaw has traditionally been thought to be highly conserved among vertebrates. However, here we show that the therian-unique face (muzzle) evolved via a drastic alteration of the common pattern of the tetrapod jaw. Through comparative morphological and developmental analyses, we demonstrated that the therian mammal's premaxilla (rostral-most upper jawbone) is derived from the maxillary prominence of the mandibular arch. The developmental primordium that produces the premaxilla in nonmammalian tetrapods rarely contributes to the upper jaw in therian mammals but rather forms a motile nose. We propose that these previously unrecognized rearrangements allowed key innovations such as the highly sensitive tactile perception and olfactory function in mammalian evolution.

Author contributions: H.H. designed research; H.H., D.K., I.W., and H.K. performed research; H.H., D.K., T.H., S.K., and H.K. analyzed data; and H.H., D.K., T.H., I.W., S.K., and H.K. wrote the paper.

The authors declare no competing interest.

This article is a PNAS Direct Submission.

[1]To whom correspondence may be addressed. Email: h-hiroki@m.u-tokyo.ac.jp.

This article contains supporting information online at http://www.pnas.org/lookup/suppl/doi:10.1073/pnas.2111876118/-/DCSupplemental.

Published October 29, 2021.

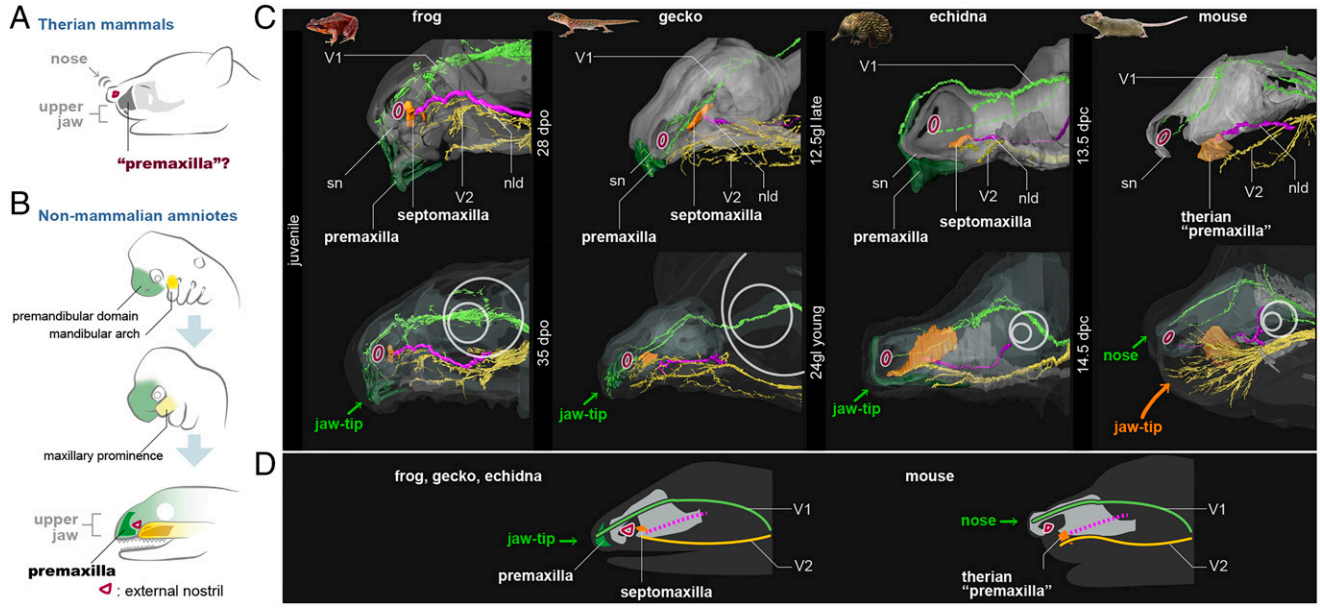

Fig. 1. Murine "premaxilla" develops differently from premaxillae of other tetrapods. (*A*) The anatomy of the therian mammal's face. (*B*) General scheme of craniofacial development in amniotes (10, 11, 15). (*C*) Three-dimensional models of tetrapod embryos. The murine premaxilla ossifies in the same topographical position as the septomaxilla (orange) of other species. The infraorbital branch (nerve branch for vibrissae) of V2 was removed in 13.5 dpc mouse. The summary is shown in *D*. sn, solum nasi; nld, nasolacrimal duct; V1, ophthalmic nerve; V2, maxillary nerve. (Not to scale.)

the chondrocranium (Fig. 1*C*). In the frog and gecko, the premaxilla grows throughout development to form the rostral end of the upper jaw, whereas in the monotreme (echidna), this bone becomes relatively smaller, and the occupying region is gradually replaced by the septomaxilla (Fig. 1*C* and *SI Appendix*, Fig. S2). In the mouse, the therian premaxilla first ossifies laterally to the nasal capsules, at the caudolateral edge of the cartilaginous narial fenestra, adjacent to the anterior opening of the nasolacrimal duct, which corresponds to features of the septomaxilla in nontherian animals. The nontherian premaxilla arises in the innervation domain of the ophthalmic nerve (V1), whereas the murine premaxilla develops in the domain of the maxillary nerve (V2). The rostral tip of the nasal cartilage, where the nontherian premaxilla occurs, does not produce any bony elements in the mouse. The V1 distribution domain does not contribute to any parts of the upper jaw in mice but rather forms the tip of the nose (*SI Appendix*, Fig. S3). Thus, the topographical position of the premaxilla conspicuously differs between the mouse and the nonmammalian tetrapods, implying that the homonymous bones may differ morphologically and/or developmentally. In particular, our comparative embryological analyses raise the possibility that the murine premaxilla more closely resembles the nontherian septomaxilla (Fig. 1*D*).

Maxillary Prominence Contributes to the Murine Premaxilla. Given that the distribution pattern of the trigeminal nerve reflects its embryonic origin, the therian premaxilla that develops in the domain of V2 may originate from the maxillary prominence of the mandibular arch. To assess this, we conducted experiments to trace the cell lineage of the maxillary prominence using *Dlx1*-CreER^{T2} mice. The *Dlx1* gene is expressed in the neural crest cells in the mandibular and posterior arches but not in the frontonasal domain, allowing the distinction of the maxillary prominence from the frontonasal domain at the pharyngula stage (*SI Appendix*, Fig. S4*A*) (16). In both *Dlx1*-CreER^{T2};R26R^{LacZ} and ;R26R^{YFP} mice, the mesenchyme of the maxillary prominence was successfully labeled from 9.5 to 10.5 dpc (days postcoitum) (*SI Appendix*, Fig. S4). The labeled cell mass protruded rostrally, eventually giving rise to the rostral-most soft tissue of the upper jaw in older embryos (Fig. 2 *A* and *B* and *SI Appendix*, Fig. S5). The distribution of the labeled cells clearly and exclusively overlapped the innervating area of V2 (Fig. 3*C* and *SI Appendix*, Fig. S5). Furthermore, in the fetal stage, the labeled cells were found in the murine premaxilla in *Dlx1*-CreER^{T2};R26R^{LacZ} mice, with the exception of the palatal process (primary palatal portion) (Fig. 3*D*). In *Dlx1*-CreER^{T2};R26R^{YFP} mice, the labeled cell mass overlapped the Runx2-positive cells in the positions of the main body of the premaxilla at 14.5 dpc, suggesting that these cells contribute to the ossification of this bone (Fig. 3*E*). In contrast to the jaw part, no labeled cells were found in the V1 domain, including the soft tissue in the nose.

These experimental results demonstrate that, unlike nonmammalian tetrapods, in the mouse, the premaxilla is derived almost entirely from the maxillary prominence. In contrast, cell lineage tracing in the chicken showed that the premaxilla is exclusively derived from the frontonasal mesenchyme (17). The present finding concurs with those for the *Ednra*$^{Edn1/+}$ transgenic mouse (18), whose maxillary prominence derivatives, including the main body of the premaxilla, partially transform into the lower jaw identity (*SI Appendix*, Fig. S6).

Inhibition of Primordial Growth. To compare which of the facial primordia gives rise to the premaxilla and septomaxilla in different amniotes, we impeded facial development. Using chicken (*Gallus gallus*) and mouse embryos, we artificially constructed cleft lip and cleft palate (cleft lip/palate) conditions with cyclopamine to inhibit the neural crest mesenchymal proliferation via the suppression of the Sonic hedgehog pathway following previously reported methods (19, 20). In the late pharyngular stages, the fusions of the frontonasal and maxillary prominences were successfully inhibited both in chicken and mouse, and clefts formed between these primordia. We also observed gecko embryos that spontaneously showed cleft lip/palate conditions.

The clefts of these three animals persisted in the same position throughout development, dividing the whole snout into three parts: two lateral maxillary prominence parts and the middle frontonasal part (Fig. 3*A*). In the chicken and gecko,

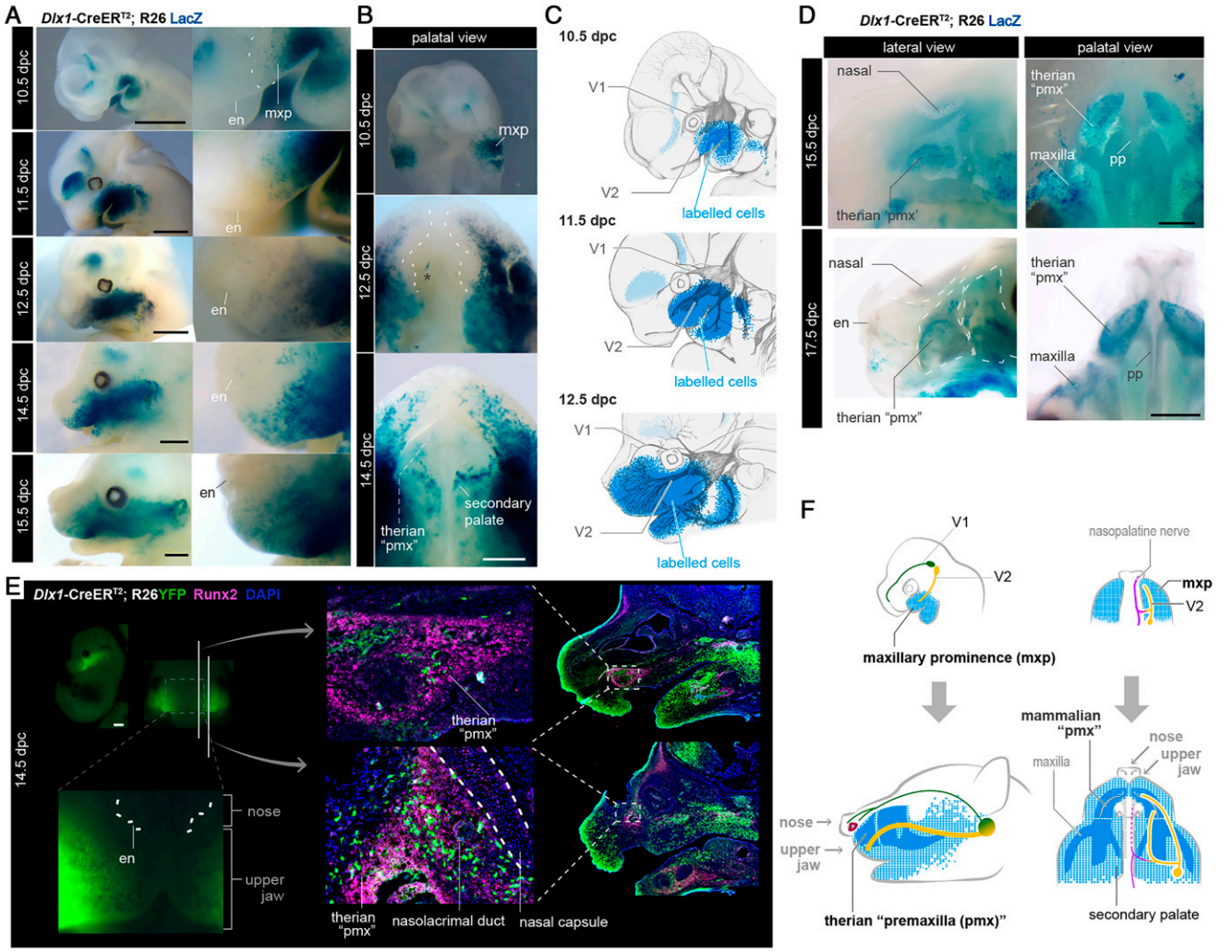

Fig. 2. Maxillary prominence contributes to the murine premaxilla. (*A–C*) *Dlx1*-CreER^{T2};R26R^{LacZ} mouse embryos with X-gal staining. Corresponding to the trigeminal nerve morphology, the labeled maxillary prominence (mxp) mesenchymal cells contribute to almost the entire upper jaw. The asterisk indicates the few cellular contaminations only around the peripheral nerve (*SI Appendix*, Fig. S5). (*D*) Labeled cells are found in the main body of the murine premaxilla. No labeled cells are found in the nasal bone. The primary palate (nasopalatine nerve domain) is also unlabeled. (*E*) The labeled cells contribute to the osteogenic region of the murine premaxilla. (*F*) The blue shading and dots indicate the distributions of the labeled cells. en, external nostril; pp, palatine process of the premaxilla; V1, ophthalmic nerve; V2, maxillary nerve. (Scale bars: 1 mm.)

the separation coincided with both the V1–V2 boundary and the premaxilla–maxilla suture, suggesting that the premaxilla is entirely derived from the frontonasal prominence, consistent with the generally accepted view (2, 4, 8, 10, 11). Another dermal element, the septomaxilla, was found in the maxillary process domain, caudolateral to the cleft in the gecko (Fig. 3*B* and *SI Appendix*, Fig. S7). In the mouse, the upper jaw was also divided into the medial and lateral components, each coinciding with the nerve distributions. Specifically, the medial component, or the palatine process, arises in the frontonasal domain. However, unlike the gecko and chicken, the main body of the premaxilla was found on the lateral side of the cleft, the domain of V2 (Fig. 3*B* and *SI Appendix*, Fig. S7). Thus, the therian premaxilla is not entirely a frontonasal derivative; instead, its main body is likely derived from the maxillary prominence (Fig. 3*C* and *SI Appendix*, Fig. S7*B*), which is equivalent to the nontherian septomaxilla. Therefore, we conclude that the therian premaxilla is a uniquely composite structure, consisting of homologs of the nonmammalian premaxilla and possibly the septomaxilla and developed from the frontonasal prominence and maxillary prominence, respectively.

Comparison of Synapsid Fossils. To understand the evolutionary history of the therian premaxilla, we examined the fossil record in the stem group of mammals, or fossil synapsids. The septomaxilla is found inside of the nostrils in many tetrapods (21–23). Indeed, septomaxilla were observed inside the nostrils of juvenile geckos and frogs (Fig. 4*A*). We confirmed that the septomaxilla was a small bony element in the nasal opening, which was pierced by the nasolacrimal duct in the basal synapsids [e.g., †*Dimetrodon* (23) and †*Dicynodontoides*; Fig. 4 *B* and *C*]. In the Gorgonopsia and Therocephalia, which are closer to the Mammalia than †*Dimetrodon*, the lateral part of the septomaxilla had begun to extend onto the lateral surface of the bony snout (Fig. 4*C* and *SI Appendix*, Fig. S8) (23–25). The premaxilla and septomaxilla remain separated in most cynodonts and mammaliaform lineages (26–36) (Fig. 4*D*). A significant change occurs in the lineage toward the Theria: the medial part of the premaxilla is lost, and a single nasal aperture appears in the osteocranium (Fig. 4*D*). Given that modern marsupials exhibit complete "therian premaxilla" like those of eutherians, the fusion of the septomaxilla (main body) and premaxilla (palatal process) should have occurred in the common ancestor of

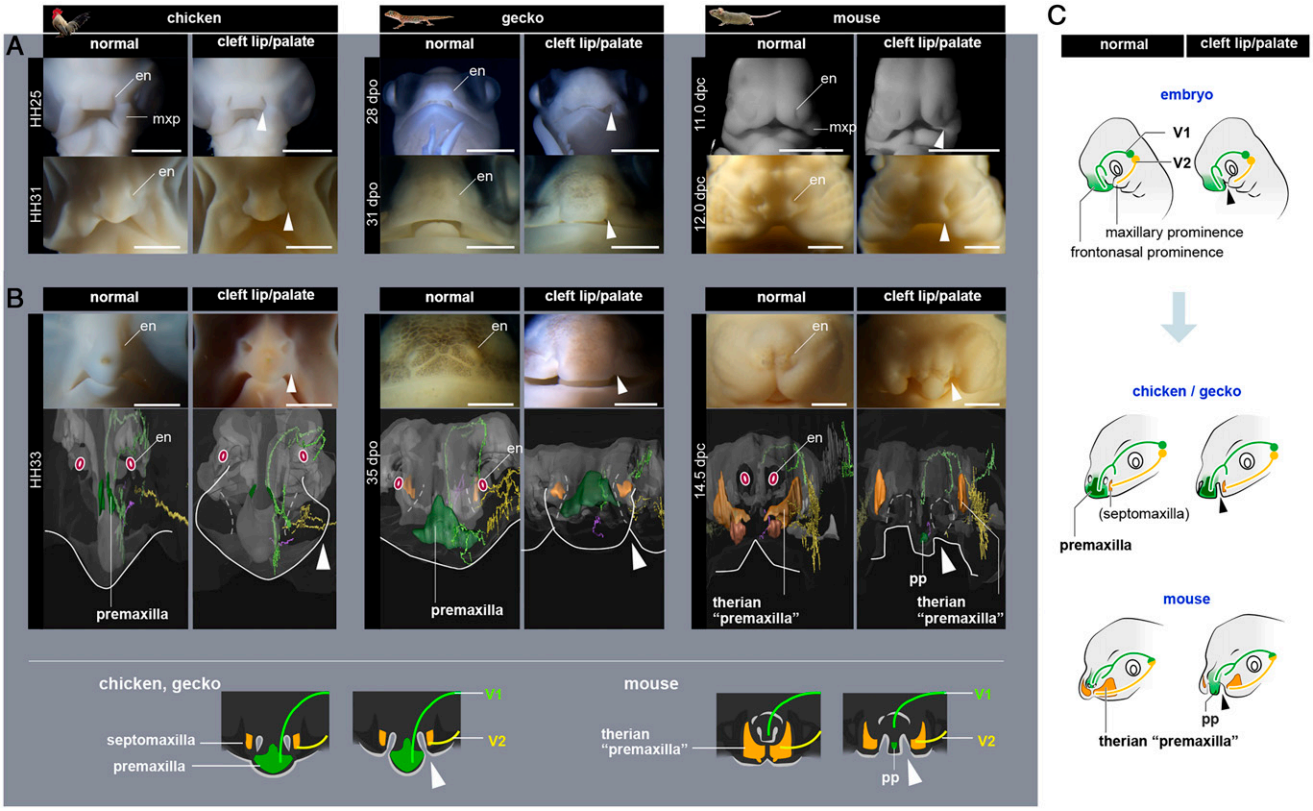

Fig. 3. The cleft lip/palate experiment reveals the distinctive embryonic origin of the therian premaxilla. (*A*) The details of the development of the normal and cleft lip/palate chicken, gecko, and mouse. The arrowheads indicate the clefts, which are found between the frontonasal and lateral maxillary primordia. (*B*) Three-dimensional models of normal and cleft lip/palate embryos. The arrowheads indicate the positions of clefts between the facial primordia. See also *SI Appendix*, Fig. S7. (*C*) Although the premaxilla is derived entirely from the frontonasal prominence (medially to the clefts) in the chicken and gecko, the murine premaxilla is lateral to the cleft, except for the small palatal process (pp). V1, ophthalmic nerve; V2, maxillary nerve. (Scale bars: 2 mm.)

therians. Thus, the typical mammalian muzzle should have arisen in a common ancestor of the Theria.

Discussion

One long-lasting enigma of comparative anatomy is that the rostral-most part of the upper jaw is innervated by different nerve branches in mammals and nonmammalian tetrapods (15). In the present study, we showed that the premaxilla of nonmammalian tetrapods is not represented in the rostral-most part of the upper jaw in therian mammals but rather forms a motile nose (Fig. 5*A*). Developmentally, the maxillary prominences on both sides circumscribe the entire upper jaw, leading to a novel configuration of the rostral-most jawbone and the rostral distribution of maxillary vibrissae accompanied by V2 (7, 37, 38) (*SI Appendix*, Fig. S9*A*). In vertebrate embryos, craniofacial primordia develop semiautonomously as developmental modules (39), each maintaining its morphological identity and topographical relationship (40, 41) with specific cranial nerve branches. Thus, the described enigma in the innervation pattern are attributable to the rearrangement of the developmental primordia and resultant reconfiguration of the premaxilla-related structures in the rostral-most part of the upper jaw in the lineage toward therian mammals.

The suggested evolutionary changes in developmental patterns can be traced in the gradual replacement of the premaxilla and septomaxilla in the series of fossil synapsids (Fig. 5*B*). This sequence is partially mirrored in the development of monotremes with the gradual loss of the prenasal part of the premaxilla and in the evolutionary fusing of septomaxilla and premaxilla in therians (Fig. 1*C* and *SI Appendix*, Fig. S2), suggesting a heterochronic change as a mode of morphological evolution. In parallel, the contribution of the other pharyngeal arch elements to the facial part of the cranium, such as the establishment of maxillary vibrissae and facial muscles, also occurred in derived synapsids (*SI Appendix*, Fig. S9) (37, 38). Thus, the fossil evidence indicates that the developmental pattern of the craniofacial primordia had uniquely changed in the evolutionary lineage toward modern mammals. Until now, the septomaxilla was regarded either to be lost in therian mammals or to remain as the os nasale only in the xenarthran mammals (e.g., armadillos) (Fig. 4*D*) (23, 24, 42, 43). A few classic histological studies, however, suggested that the septomaxilla had been fused into the therian premaxilla during evolution (44). Our results revive this old hypothesis: the main body of the therian premaxilla should be homologous with the nonmammalian septomaxilla. Indeed, the therian premaxilla develops from two separate ossification centers—the facial part and the palatal process—in many species (7, 23, 45), which is consistent with our findings.

In conclusion, the mammalian muzzle can be assigned as an evolutionary novelty (46) explained by a disruption of the ancestral morphological network (i.e., morphological homologies) and the establishment of new connections of modules. Namely, the mammalian maxillary prominence has invaded into the teeth-forming field of the rostral-most region of the upper jaw (ancestrally occupied by the premandibular domain), resulting in the unique incisor-bearing septomaxilla, an element not found in any other tetrapods. This reduction of the ancestral premaxilla and recruitment of the septomaxilla in the

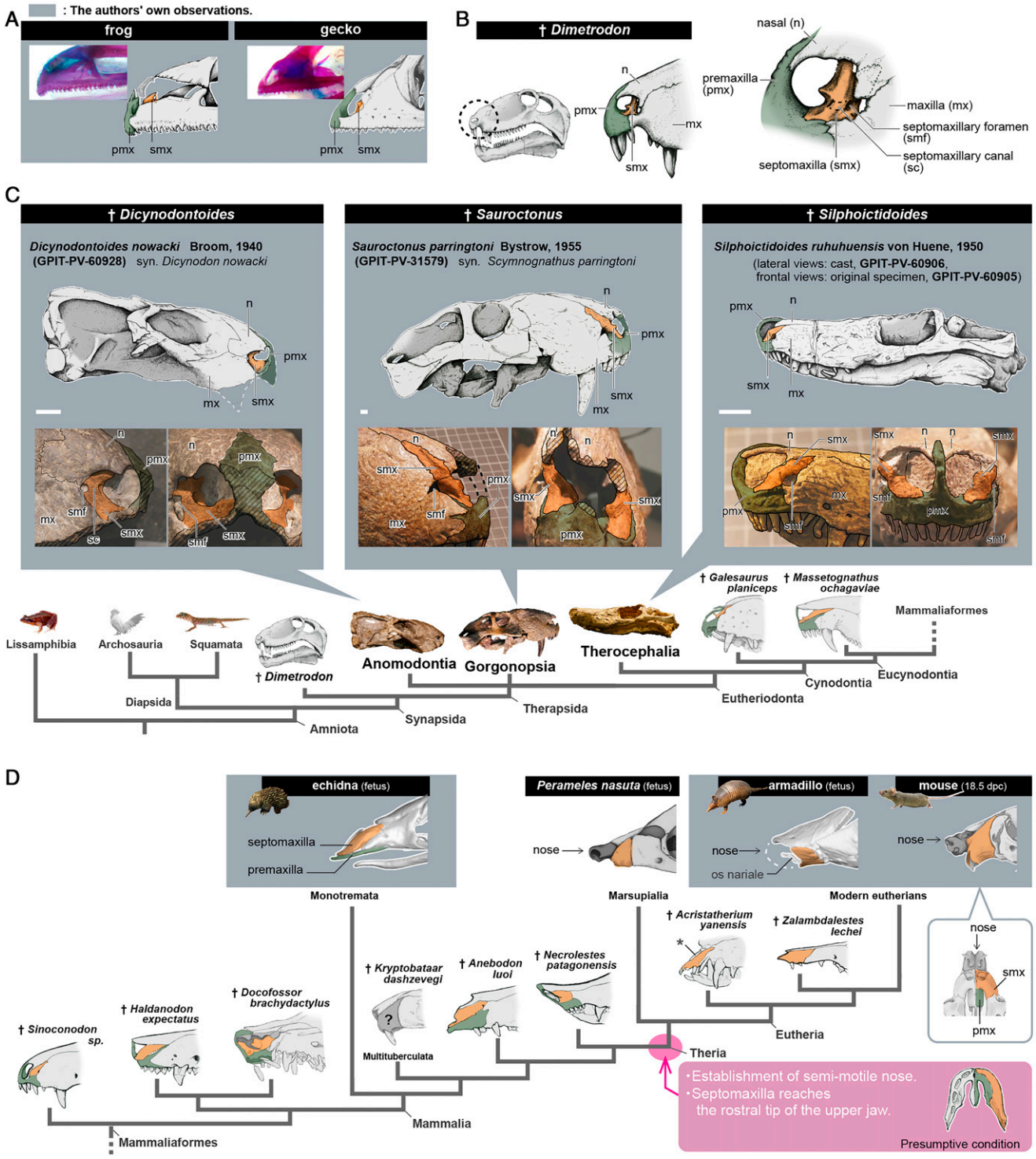

Fig. 4. Evolutionary transitions of upper jaw bones in the fossil synapsids. (*A*) Upper jaw skeleton of the frog and gecko. (*B*) The snout of †*Dimetrodon*, which was redrawn from the previous study (23). The septomaxilla is housed in the nostril. (*C*) The observation of fossil synapsids. The †*Silphoictidoides* fossil shows a large septomaxilla covering the rostral surface of the snout, the proportions of which resemble those of the embryonic echidna (Fig. 1*C* and *SI Appendix*, Fig. S2). The phylogenetic framework is based on a previous study (25). The schemes of cynodonts were redrawn from previous studies: †*Galesaurus planiceps* (flipped left to right from the original figure) (26), †*Massetognathus ochagaviae* (27). (*D*) The transition of upper jaw bones in the Mammaliaformes. Some old studies identified the os nasale of the xenarthran mammals as the septomaxilla homolog, but this bone is likely a neomorph of xenarthrans as discussed in recent studies (23, 28). Similarly, the bony element (asterisk) found in the snout of the stem-eutherian †*Acristatherium* (29) should not be homologous with the septomaxilla. Although the "premaxilla" of the Multituberculata (dark gray) is quite similar to the therian premaxilla, it is currently impossible to exclude the possibility that the multituberculates' "premaxilla" incorporated a neomorphic bone rather than a homolog of the septomaxilla without minute analyses of topographical position of the soft tissues. The schemes were redrawn from previous studies: *Perameles nasuta* (30), †*Sinoconodon sp* (31), †*Haldanodon expectatus* (32), †*Docofossor brachydactylus* (flipped left to right from the original figure) (33), †*Kryptobaatar dashzevegi* (34), †*Anebodon luoi* (35), †*Necrolestes patagoniensis* (28), †*Acristatherium yanensis* (29), and †*Zalambdalestes lechei* (36). The phylogenetic framework is based on refs. 26 and 29. mx, maxilla; n, nasal; pmx, premaxilla; sc, septomaxillary canal; smf, septomaxillary foramen; smx, septomaxilla. (Scale bars: 2 cm.)

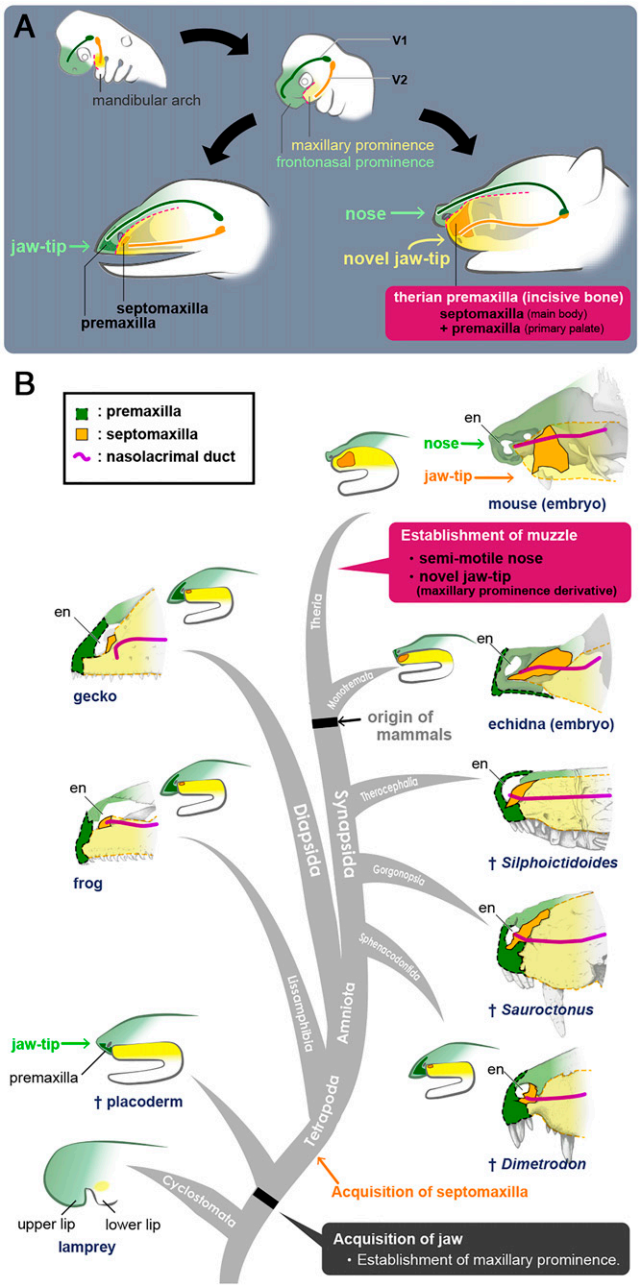

Fig. 5. Evolution of the mammalian muzzle. (*A*) The developmental scheme of the nontherian amniotes and therian mammals. (*B*) Simplified evolutionary scenario of the vertebrate snout. In plesiomorphic condition, the premandibular mesenchyme (light green) comprises the rostral-most part of the oral apparatus, and it has been strongly conserved in the crown vertebrates (cyclostomes and gnathostomes) (11, 12). However, this persistent conservativeness had gradually been remodeled to bring about a novel pattern in the synapsid lineage.

mammalian upper jaw could have served as a key innovation that permitted the evolution of the semimotile nose unique to therians, adding to the expansion of facial muscles that characterize all mammals. Thus, the embryonic reconstitution of the mammalian muzzle, including the upper jaw and nose, is another novel evolutionary feature, similar to classic examples such as the mammalian middle ear (4, 47–49) or the turtle shell (50). Our present study on the therian premaxilla, or incisive bone, gives a fresh perspective on the premaxilla, whose homology has not been questioned since the dawn of comparative morphology (9). This finding provides a basis for studies of the evolution of the mammalian muzzle as well as a reconsideration of the traditional framework of craniofacial morphology of jawed vertebrates.

Materials and Methods

Laboratory Animal Specimens. Procedures involving animals were approved by the University of Tokyo Animal Care and Use Committee (approval identification: P14-109, P16-071, P19-043, and P19-050) and the guidelines of the RIKEN Center for Developmental Biology. For the present study, we used the embryos of mice, chickens, geckos, and frogs.

For mice (*Mus musculus*), we used two wild-type strains (C57BL/6J and ICR) as well as *Dlx1*-CreER^{T2}, Rosa26R$^{LacZ/LacZ}$, and Rosa26R$^{YFP/YFP}$ mice. All these strains were kept in the laboratory at the University of Tokyo. The mice were housed in light-, temperature- (25 °C), and humidity-controlled conditions, and food and water were available ad libitum. We also revalidated data of *Ednra*$^{Edn1/+}$ mice skulls that were obtained in our laboratory in 2008 (*SI Appendix*, Fig. S6). See the following sections for details of the genetic experiments.

For chicken (*Gallus gallus*), we incubated fertilized eggs of the Boris Brown chicken in a humidity chamber at 38 °C, and the embryos were staged according to Hamburger and Hamilton criteria (51).

For the gecko (Madagascar ground gecko, *Paroedura picta*), we collected fertilized eggs of the Madagascar ground gecko in 2012 from the Laboratory for Animal Resources and Genetic Engineering, RIKEN Center for Developmental Biology. They were incubated in a humidity chamber at 38 °C. The embryos were staged according to Noro et al. (52).

For the frog (Japanese brown frog, *Rana japonica*), we obtained fertilized eggs legally from a rice field in Shibasaki, Tsukuba, Ibaraki Prefecture, Japan, in May 2018. The eggs were kept in a tank with fresh water. We fed spinach leaves to the hatched tadpoles and fixed the animals during the metamorphosis stage.

Museum Specimens. For the study of the short-beaked echidna (*Tachyglossus aculeatus*), we observed and took high-resolution photos of three histological sections from the Hill Collection at the Berlin Museum of Natural History: 1) *Tachyglossus aculeatus* MO55, 8 greatest length (gl) p egg 14.5 mm; 2) *Tachyglossus aculeatus* M158, 12.5 gl late-stage p egg 17 mm; and 3) *Tachyglossus aculeatus* M161, 24 gl p young stage.

We examined five fossil samples from the Paleontological Collection of the Eberhard Karls Universität: 1) *Dicynodontoides nowacki* Broom, 1940. syn. *Dicynodon nowacki* (Huene, 1942) (GPIT-PV-60928, syn. GPIT/RE/7173); 2) *Sauroctonus parringtoni* Bystrow, 1955. syn. *Scymnognathus parringtoni* Huene, 1950 (GPIT-PV-31579, syn. GPIT/RE/7113); 3) *Dinogorgon rubidgei* Broom, 1936. syn. *Dinogorgon quinquemolaris* Huene, 1950 (GPIT-PV-116184, syn. GPIT/RE/7114); 4); *Silphoictidoides ruhuhuensis* von Huene, 1950 (GPIT-PV-60905 and its cast, GPIT-PV-60906, syn. GPIT/RE/7138A); and 5) *Theriognathus microps* Owen, 1876. syn. *Notosollasia luckoffi* Broom, 1936 (GPIT-PV-60909, syn. GPIT/RE/7142). We also observed 6) *Dimetrodon sp.* (GPIT-PV-40976) to draw the whole image of the skull.

We also used two legally collected, alcohol-preserved specimens: 1) armadillo (*Dasypus hybridus*), UMUT14772, CRL 80 mm from the University Museum of the University of Tokyo and 2) echidna, ZMB echidna 81, CRL 43 mm from the Museum für Naturkunde, Berlin, Germany.

The *Dlx1*-CreERT2 Mouse Experiment. The B6;129S4-*Dlx1* < tm1(cre/ERT2)Zjh>/J(*Dlx1*-CreER^{T2}) adult mice were purchased from The Jackson Laboratory through Charles River Laboratories Japan and maintained with a mixed (C57BL6/ICR) genetic background through heterozygous mating. For cell lineage tracing, we paired *Dlx1*-CreER^{T2} mice with R26R$^{LacZ/LacZ}$ or R26R$^{YFP/YFP}$ mice. Cre recombinase activity was induced via oral administration of tamoxifen (Sigma-Aldrich, no. T5648) in corn oil (Sigma-Aldrich, no. C8267) at a dose of 0.1 mg/g body weight. The administration was performed once at 8.5, 9.5, and 10.5 dpc, and mice administered at 9.5 dpc were used for the analysis (*SI Appendix*, Fig. S5). Embryos from stages 10.5 to 17.5 dpc were collected. We tested at least four mothers at each stage.

β-galactosidase Detection. Embryos were fixed in 4% paraformaldehyde (PFA) in 0.1 M phosphate-buffered saline (PBS) with 0.2% glutaraldehyde containing 5 mM ethylene glycol tetraacetic acid and 2 mM $MgCl_2$ at 4 °C for 15 min. They were then washed with a washing buffer (2 mM $MgCl_2$, 0.02% Nonidet P-40, and 0.1% sodium deoxycholate in PBS) three times for 30 min each time. Next, embryos were preincubated in a 0.2-M kaolinite phenylphosphonate (KPP) solution (a mixture of 0.1 M KH_2PO_4 and 0.1 M K_2HPO_4 to which

was added 2 mM $MgCl_2$, 0.02% Nonidet P-40 and 0.1% sodium deoxycholate immediately before use) for 10 min and then incubated in the stain solution of 10 mM $K_3[Fe(CN)_6]$, 10 mM $K_4[Fe(CN)_6]$, and 1 mg/mL X-gal (Cayman Chemical, no. 16495) in KPP solution in darkness overnight at 37 °C. After staining, the samples were washed with PBS and postfixed using 4% PFA/PBS.

Cleft Lip/Palate Preparation. For the mouse, as described by Lipinski et al. (20), we administered cyclopamine through subcutaneous implantation of a micro-osmotic pump. The cyclopamine (LC Laboratories, no. C-8700) was dissolved in a sodium phosphate/citrate buffer containing 2-hydropropyl-b-cyclodextrin (HPBCD) (Sigma-Aldrich) shortly before use; the amount used was 1.5 mg cyclopamine/100 μL 30% HPBCD (percentage by weight). Then, the solution was injected into the micro-osmotic pump (Alzet, no. 2001D), and the implantation was conducted at 8.25 dpc. The same cyclopamine solution was used for the chicken. We injected 10 to 30 mL solution into the perifacial region of stage 15 chicken embryos following the method used by Abzhanov et al. (19). For the gecko, we occasionally obtained wild-type cleft lip/palate embryos.

Whole-Mount Immunohistochemistry. To visualize the peripheral nerve in mice, we used monoclonal antibody 2H3 (Developmental Studies Hybridoma Bank, University of Iowa). The embryos were fixed with 4% PFA/PBS, washed and dehydrated in a graded series of methanol (70%, 95%), and stored at −30 °C. Next, they were placed into a mixture of hydrogen peroxide and methanol (1:9) for several days for depigmentation and for blocking endogenous peroxidase activities. Then, 0.5 mL 10% Triton X-100 in distilled water was added, and the embryos were further incubated for 30 min at room temperature. After washing in Tris HCl–buffered saline solution (TST: 20 mM Tris HCl [pH 8.0], 150 mM NaCl, 0.01% Triton X-100), the samples were blocked with 5% nonfat dried milk in TST (TSTM). The embryos were then incubated in a primary antibody solution (diluted 1/100 in spin-clarified TSTM containing 0.1% sodium azide) for 2 to 4 d at 37 °C while being gently agitated. The secondary antibody used was horseradish peroxidase (HRP)-conjugated polyclonal goat anti-mouse (Dako, no. P0447) diluted 1/400 in TSTM. After the final wash in TST, the embryos were incubated with peroxidase substrate 3,3′-diaminobenzidine (100 μg/mL) in TST with 0.01% (vol/vol) hydrogen peroxide (35% aqueous solution) for 20 to 40 min.

Skeletal Preparation. The skeletal staining of embryos was conducted using Alizarin red and Alcian blue solutions. Samples were fixed in 95% ethanol for 1 wk, placed in acetone for 2 d, and then incubated with 0.015% Alcian blue 8GS, 0.005% Alizarin red S, and 5% acetic acid in 70% ethanol for 3 d. After washing in distilled water, the samples were cleaned in 1% potassium hydroxide for several days and in clear, unobstructed, brain imaging mixtures solutions (53) until the surrounding tissues turned transparent.

Histological Sections. The embryos were fixed in modified Serra's fixative (4% PFA containing ethanol and acetic acid), dehydrated, and embedded in paraffin wax. Sections were cut at a thickness of 6 to 10 μm, depending on the size of the embryos. To visualize the nerve axons, we conducted immunohistochemistry. For the chicken, gecko, and frog embryos, the primary antibody used was CD57 (HNK-1, Becton, Dickinson and Co., no. 347390), and the secondary one was HRP-conjugated goat anti-mouse immunoglobulin M (Santa Cruz Biotechnology, no. sc-2064). For the mice embryos, we used anti-acetylated tubulin (Sigma-Aldrich, no. T7451) and HRP-conjugated polyclonal goat anti-mouse (Dako, no. P0447). Then, the sections were also stained with Alcian blue, hematoxylin, and eosin following standard protocols.

Three-Dimensional Imaging. For three-dimensional reconstruction, the stained sections of the embryos were digitized using an Olympus BX60 microscope equipped with an Olympus DP70 camera and Olympus DP controller software (Olympus). On the digitized sections, each embryonic component was identified and reconstructed using the AMIRA 3D Visualization Framework (Thermo Fisher Scientific).

Frozen Sections and Fluorescent Immunohistochemistry. We conducted fluorescent observations of the *Dlx1*-CreER^{T2};R26R$^{YFP/YFP}$ mouse embryos. The embryos were trimmed and fixed for 2 h in 4% PFA/PBS. They were then successively soaked in a 15 to 30% sucrose gradient and embedded in Optimal Cutting Temperature Compound (Tissue Tek, Sakura Finetek) for frozen sections. Sections with a thickness of 10 μm were made using a CryoStar NX70 (Thermo Fisher Scientific). To visualize the yellow fluorescent protein (YFP) signals, we conducted immunohistochemistry using monoclonal anti–green fluorescent protein (Nacalai, no. 04404) as the primary antibody and donkey anti-rat IgG H&L (Alexa Fluor 488; Abcam, no. ab150153) as the secondary antibody. We also used anti-Runx2 (Abcam, no. ab23981) and goat anti-rabbit IgG H&L (Alexa Fluor 555; Abcam, no. ab150078). Finally, the sections were stained with 4',6-diamidino-2-phenylindole and observed with a fluorescence microscope (Keyence, no. BZ-X710).

Whole-Mount In Situ Hybridization. Digoxigenin (DIG)–labeled riboprobes for *Dlx1* mice were generated using a DIG RNA labeling kit (Roche). Whole-mount in situ hybridization was performed as previously described (47).

Microcomputerized Tomography Scans. We acquired grayscale images of museum fetal specimens (UMUT14772 and ZMB echidna 81) using a microfocal X-ray CT inspeXio SMX-90CT Plus system at the Musashino Art University (Shimadzu) with 90 kV source voltage and 100 μA source currents. Slice thickness ranged from 13 to 36 μm. Each of the reconstructed images was in the form of 1,024 × 1,024 matrices of 12-bit greyscale values. Manual segmentation and analysis of greyscale images were conducted in Amira 5.2 (Visage Imaging).

Data Availability. All study data and materials are available as described in the article and/or *SI Appendix*.

ACKNOWLEDGMENTS. We greatly appreciate Peter Giere (Museum für Naturkunde, Berlin) for supporting our observation of the historical echidna sections in the Hill Collection. We are also grateful to Yukiko Kurihara and Akiyasu Iwase (The University of Tokyo) for technical advice with mouse experiments and for help with keeping mice; Kaoru Mizukami and Yuka Haneda (The University of Tokyo) for helping with frog and chicken experiments; Giovanni Levi (Muséum National d'Histoire Naturelle, Paris), Masaki Takechi (Tokyo Medical Dental University), Daichi G. Suzuki (The University of Tsukuba), Takao K. Suzuki (The University of Tokyo), and Mikiko Tanaka (Tokyo Institute of Technology) for technical and scientific advice; Kai Ito (Tsurumi University) and Kengo Iwai (Musashino Art University) for helping with three-dimensional reconstructions; and Yuriko Kondo (The University of Tokyo) for secretarial assistance. We acknowledge financial support from Japan Society for the Promotion of Science (JSPS) Grants 17J11177, 20H04858, 20K15858 (H.H.), 18H04816, 18H02492, 18K19359, and 18KK0207; JSPS Joint Research Program implemented in association with German Research Foundation (JRPs-LEAD with DFG) Grant JPJSJRP20181608; and City University of Hong Kong Start-up Grant 9610466 (D.K.); and DFG no. WE 5440/6-1 (I.W., D.K.). This work was also supported by JSPS Grant 15H02416, Grant-in-Aid for Scientific Research on Innovative Areas (Research in a Proposed Research Area) 17H06385, and a Naito Grant for the Promotion of Focused Research (S.K.) and JSPS Grant 19H01048 and Core Research for Evolutional Science and Technology of the Japan Science and Technology Agency Grant JPMJCR13W2 (H.K.).

1. E. M. Hemingway, *For Whom the Bell Tolls*, S. Wood, director (motion picture, Paramount Pictures, 1943).
2. A. S. Romer, T. S. Parsons, *The Vertebrate Body* (Saunders College, Philadelphia, ed. 6, 1986).
3. T. S. Kemp, *The Origin and Evolution of Mammals* (Oxford University Press, 2005).
4. K. V. Kardong, *Vertebrates: Comparative Anatomy, Function, Evolution* (McGraw-Hill, ed. 5, 2008).
5. T. B. Rowe, T. E. Macrini, Z. X. Luo, Fossil evidence on origin of the mammalian brain. *Science* **332**, 955–957 (2011).
6. A. Crompton, C. Musinsky, T. Owerkowicz, "Evolution of the mammalian nose" in *Great Transformations in Vertebrate Evolution*, K. P. Dial, N. Shubin, E. L. Brainerd, Eds. (University of Chicago Press, 2015), pp. 189–203.
7. W. Maier, A neglected part of the mammalian skull: The outer nasal cartilages as progressive remnants of the chondrocranium. *Vertebr. Zool.* **70**, 367–382 (2020).
8. S. G. de Beer, *The Development of the Vertebrate Skull* (Clarendon Press, 1937).
9. J. W. von Goethe, Über den Zwischenkiefer der Menschen und der Tiere *Verhandlungen der Kaiserlich Leopoldinisch-Carolinischen Akademie der Naturforscher* Bd.7, 1–48 (1831). (Original work published 1786).
10. F. Santagati, F. M. Rijli, Cranial neural crest and the building of the vertebrate head. *Nat. Rev. Neurosci.* **4**, 806–818 (2003).
11. S. Kuratani, Evolution of the vertebrate jaw from developmental perspectives. *Evol. Dev.* **14**, 76–92 (2012).
12. V. Dupret, S. Sanchez, D. Goujet, P. Tafforeau, P. E. Ahlberg, A primitive placoderm sheds light on the origin of the jawed vertebrate face. *Nature* **507**, 500–503 (2014).
13. M. Zhu *et al.*, A Silurian placoderm with osteichthyan-like marginal jaw bones. *Nature* **502**, 188–193 (2013).
14. M. Zhu *et al.*, A Silurian maxillate placoderm illuminates jaw evolution. *Science* **354**, 334–336 (2016).
15. H. Higashiyama, S. Kuratani, On the maxillary nerve. *J. Morphol.* **275**, 17–38 (2014).

16. M. J. Depew, T. Lufkin, J. L. Rubenstein, Specification of jaw subdivisions by *Dlx* genes. *Science* **298**, 381–385 (2002).
17. S. H. Lee, O. Bédard, M. Buchtová, K. Fu, J. M. Richman, A new origin for the maxillary jaw. *Dev. Biol.* **276**, 207–224 (2004).
18. T. Sato *et al.*, An endothelin-1 switch specifies maxillomandibular identity. *Proc. Natl. Acad. Sci. U.S.A.* **105**, 18806–18811 (2008).
19. A. Abzhanov, D. R. Cordero, J. Sen, C. J. Tabin, J. A. Helms, Cross-regulatory interactions between *Fgf8* and *Shh* in the avian frontonasal prominence. *Congenit. Anom. (Kyoto)* **47**, 136–148 (2007).
20. R. J. Lipinski *et al.*, Dose- and route-dependent teratogenicity, toxicity, and pharmacokinetic profiles of the hedgehog signaling antagonist cyclopamine in the mouse. *Toxicol. Sci.* **104**, 189–197 (2008).
21. J. A. Clack, A. C. Milner, *Handbook of Paleoherpetology, Part 3A1: Basal Tetrapoda* (Verlag Dr. Friedrich Pfeil, 2015).
22. I. I. Schmalhausen, *The Origin of Terrestrial Vertebrates* (Academic Press, New York, 1968).
23. J. R. Wible, D. Miao, J. A. Hopson, The septomaxilla of fossil and recent synapsids and the problem of the septomaxilla of monotremes and armadillos. *Zool. J. Linn. Soc.* **98**, 203–228 (1990).
24. W. J. Hillenius, Septomaxilla of nonmammalian synapsids: Soft-tissue correlates and a new functional interpretation. *J. Morphol.* **245**, 29–50 (2000).
25. K. D. Angielczyk, C. F. Kammerer, "Non-mammalian synapsids: The deep roots of the mammalian family tree" in *Mammalian Evolution, Diversity and Systematics*, F. E. Zachos, Ed. (De Gruyter, 2018), pp. 117–198.
26. L. C. Pusch, C. F. Kammerer, J. Fröbisch, Cranial anatomy of the early cynodont *Galesaurus planiceps* and the origin of mammalian endocranial characters. *J. Anat.* **234**, 592–621 (2019).
27. J. Liu, M. B. Soares, M. Reichel, *Massetognathus* (Cynodontia, Traversodontidae) from the Santa Maria Formation of Brazil. *Rev. Bras. Paleontol.* **11**, 27–36 (2008).
28. J. R. Wible, G. W. Rougier, Craniomandibular anatomy of the subterranean meridiolestidan *Necrolestes patagonensis* Ameghino, 1891 (Mammalia, Cladotheria) from the early Miocene of Patagonia. *Ann. Carnegie Mus.* **84**, 183–253 (2017).
29. Y. Hu, J. Meng, C. Li, Y. Wang, New basal eutherian mammal from the Early Cretaceous Jehol biota, Liaoning, China. *Proc. Biol. Sci.* **277**, 229–236 (2010).
30. P. C. Esdaile, On the structure and development of the skull and laryngeal cartilages of *Perameles*, with notes on the cranial nerves. *Philos. Trans. R. Soc. Lond. B Biol. Sci.* **207**, 439–479 (1916).
31. A. W. Crompton, Z. Luo, "Relationships of the Liassic mammals *Sinoconodon, Morganucodon oehleri*, and *Dinnetherium*" in *Mammal Phylogeny*, F. S. Szalay, Ed. (Springer, 1993), pp. 30–44.
32. J. A. Lillegraven, G. Krusat, Cranio-mandibular anatomy of *Haldanodon exspectatus* (Docodonta; Mammalia) from the Late Jurassic of Portugal and its implications to the evolution of mammalian characters. *Rocky Mountain Geol.* **28**, 39–138 (1991).
33. Z.-X. Luo *et al.*, Mammalian evolution. Evolutionary development in basal mammaliaforms as revealed by a docodontan. *Science* **347**, 760–764 (2015).
34. J. R. Wible, G. W. Rougier, Cranial anatomy of *Kryptobaatar dashzevegi* (Mammalia, Multituberculata), and its bearing on the evolution of mammalian characters. *Bull. Am. Mus. Nat. Hist.* **247**, 1–124 (2000).
35. S. Bi *et al.*, A new symmetrodont mammal (Trechnotheria: Zhangheotheriidae) from the Early Cretaceous of China and trechnotherian character evolution. *Sci. Rep.* **6**, 26668 (2016).
36. J. R. Wible, M. J. Novacek, G. W. Rougier, New data on the skull and dentition in the Mongolian Late Cretaceous eutherian mammal *Zalambdalestes. Bull. Am. Mus. Nat. Hist.* **281**, 1–144 (2004).
37. J. Benoit, P. R. Manger, B. S. Rubidge, Palaeoneurological clues to the evolution of defining mammalian soft tissue traits. *Sci. Rep.* **6**, 25604 (2016).
38. J. Benoit *et al.*, The evolution of the maxillary canal in Probainognathia (Cynodontia, Synapsida): Reassessment of the homology of the infraorbital foramen in mammalian ancestors. *J. Mamm. Evol.* **27**, 329–348 (2020).
39. G. Schlosser, "The role of modules in development and evolution" in *Modularity in Development and Evolution*, G. Schlosser, G. Wagner, Eds. (The University of Chicago Press, 2004), pp. 519–582.
40. G. Saint-Hilaire, *Philosophie Anatomique* (J. B. Baillière, vol. **1**, 1818).
41. A. Remane, *Die Grundlagen des natürlichen Systems, der vergleichenden Anatomie und der Phylogenetik: Theoretische Morphologie und Systematik I. Zweite Auflage* (Geest & Portig K.-G., 1956).
42. R. Wegner, Der Stützknochen, Os nariale, in der Nasenhöhle bei den Gürteltieren, Dasypodidae, und seine homologen Gebilde bei Amphibien, Reptilien und Monotremen. *Morph. Jb.* **51**, 413–492 (1922).
43. U. Zeller, J. R. Wible, M. Elsner, New ontogenetic evidence on the septomaxilla of *Tamandua* and *Choloepus* (Mammalia, Xenarthra), with a reevaluation of the homology of the mammalian septomaxilla. *J. Mamm. Evol.* **1**, 31–46 (1993).
44. E. Gaupp, Neue Deutungen auf dem Gebiete der Lehre vom Säugetierschädel. *Anat. Anz.* **27**, 273–310 (1905).
45. W. Parker, On the structure and development of the skull in the Mammalia. Part II: Edentata. *Proc. R. Soc. Lond.* **37**, 78–82 (1884).
46. G. B. Müller, G. P. Wagner, Novelty in evolution - Restructuring the concept. *Annu. Rev. Ecol. Syst.* **22**, 229–256 (1991).
47. T. Kitazawa *et al.*, Developmental genetic bases behind the independent origin of the tympanic membrane in mammals and diapsids. *Nat. Commun.* **6**, 6853 (2015).
48. A. S. Tucker, Major evolutionary transitions and innovations: The tympanic middle ear. *Philos. Trans. R. Soc. Lond. B Biol. Sci.* **372**, 20150483 (2017).
49. D. J. Urban *et al.*, A new developmental mechanism for the separation of the mammalian middle ear ossicles from the jaw. *Proc. Biol. Sci.* **284**, 20162416 (2017).
50. H. Nagashima *et al.*, Evolution of the turtle body plan by the folding and creation of new muscle connections. *Science* **325**, 193–196 (2009).
51. V. Hamburger, H. L. Hamilton, A series of normal stages in the development of the chick embryo. *J. Morphol.* **88**, 49–92 (1951).
52. M. Noro, A. Uejima, G. Abe, M. Manabe, K. Tamura, Normal developmental stages of the Madagascar ground gecko *Paroedura pictus* with special reference to limb morphogenesis. *Dev. Dyn.* **238**, 100–109 (2009).
53. E. A. Susaki *et al.*, Whole-brain imaging with single-cell resolution using chemical cocktails and computational analysis. *Cell* **157**, 726–739 (2014).